LANGMUIR Article
Cite This: Langmuir 2019, 35, 2580−2586
pubs.acs.org/Langmuir

Stabilizing Pt Nanocrystals Encapsulated in N-Doped Carbon as Double-Active Sites for Catalyzing Oxygen Reduction Reaction

Jing Liu,[†] Wenqiang Li,[†] Ruilin Cheng,[†] Qian Wu,[†] Jiahuan Zhao,[†] Daping He,[†,‡] and Shichun Mu*[,†]

[†]State Key Laboratory of Advanced Technology for Materials Synthesis and Processing and [‡]Hubei Engineering Research Center of RF-Microwave Technology and Application, Wuhan University of Technology, 430070 Wuhan, China

Supporting Information

ABSTRACT: Polypropylene fiber, a cheap source of nitrogen-doped carbon, is introduced to design robust nitrogen-doped carbon-encapsulated small Pt nanocrystals with Pt and nitrogen−carbon double-active centers toward oxygen reduction reaction (ORR). Ascribed to the separation effect of the polypropylene fiber, even suffering from a high-temperature carbonization treatment at 720 °C for 90 min, the polypropylene fiber-derived carbon-encapsulated Pt nanocrystal maintains a small particle size (3 nm diameter on average). As expected, its ORR mass activity is up to 116.5 mA/mg at 0.9 V. After 8000 cycles, the half-wave potential of the prepared catalyst declines only by 14 mV compared with 43 mV for the commercial Pt/C catalyst. The significantly improved electrochemical properties of the as-prepared catalyst are resulted from the nitrogen-doped carbon-encapsulated Pt nanocrystal structure, which is benefited to adsorption and activation of oxygen due to the presence of nitrogen-doped carbon as the important active site for ORR besides Pt metal. In addition, the migration, aggregation, and growth of Pt nanoparticles are prohibited in terms of the outer nitrogen-doped carbon protection layer, greatly enhancing the stability of the catalyst.

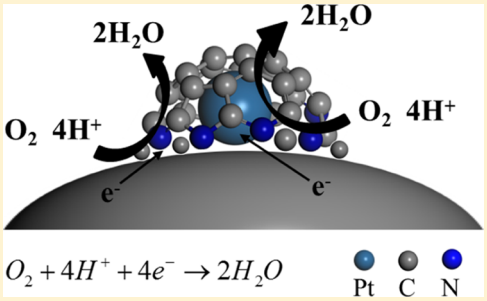

1. INTRODUCTION

Facing increasing energy contradiction and environmental issues, the development and utilization of clean energy is imperative. Because of simple structures, fast start-up speed, lower working temperatures, high energy conversion efficiency, almost no emission, and silence properties, proton exchange membrane fuel cells (PEMFCs) have been favored by researchers.[1,2] However, some factors such as high cost and low longevity of PEMFCs, which can be substantially blamed on the use of expensive and unstable platinum (Pt)-based catalysts, still restrict their commercialization. Undoubtedly, as an important component of PEMFCs, the electrochemical activity and service life of Pt-based catalysts directly affect the performance of fuel cells.

Compared to the hydrogen oxidation reaction at the anode, the oxygen reduction reaction (ORR) occurring at the cathode is a very slow kinetic process,[3,4] which becomes the rate-deciding step of the fuel cell reaction. The currently widely used catalyst at the cathode is the Pt/C catalyst,[5] wherein Pt nanoparticles (NPs) are uniformly dispersed on carbon nanospheres (such as nanosized carbon black). Although such catalysts exhibit excellent electrochemical activity during ORR, their inadequacies,[6−11] such as the extremely poor abundance as precious metal on earth and low operating lifetime in harsh environments (high humidity, strong acid, high potentials, etc.), severely weaken the performance of PEMFCs. Thus, further increasing the stability of Pt-based catalysts with maintained activity and reduced Pt dosage has become an urgent research task.

Various methods have been proposed to keep the stability of Pt-based catalysts with minimum activity loss mainly caused by dissolution, detachment, or aggregation of Pt NPs on supports. For instance, the strategies of using more stable support materials[1,12−14] and reinforcing the interaction of metal−carrier[15] have been reported. Also, Pt alloying with other elements[16−18] and structure or morphology designing[19−21] (e.g., special nanocage[22]) have been probed. Our group previously has done considerable research studies on polymer-stabilized Pt-based catalysts.[14,23−25] Pt NPs are encapsulated in the ultrathin perfluorosulfonic acid (Nafion) or polyaniline (PANI) layers, ensuring the enhanced metal−support interaction. Recently, to further increase the stability of catalysts, the polymer stabilizer can be further carbonized.[26] However, to a certain extent the surface-active sites of Pt NPs would be covered by the formed polymer layer or the carbon protective layer. In addition, the high-temperature carbonization process also accelerates the growth of Pt NPs, lowering the active surface of Pt catalysts.

Recent studies have shown that heteroatoms (such as nitrogen,[4] phosphorus,[27] sulfur,[23] etc.) have a great influence on the catalytic properties. Especially, the N-doped carbon with pyridinium nitrogen can change the charge distribution of carbon surfaces, favorable for the adsorption and activation of oxygen, promoting the ORR process.[2,12,28] At the same time,

Received: November 26, 2018
Revised: January 23, 2019
Published: January 25, 2019

DOI: 10.1021/acs.langmuir.8b03947
Langmuir 2019, 35, 2580−2586

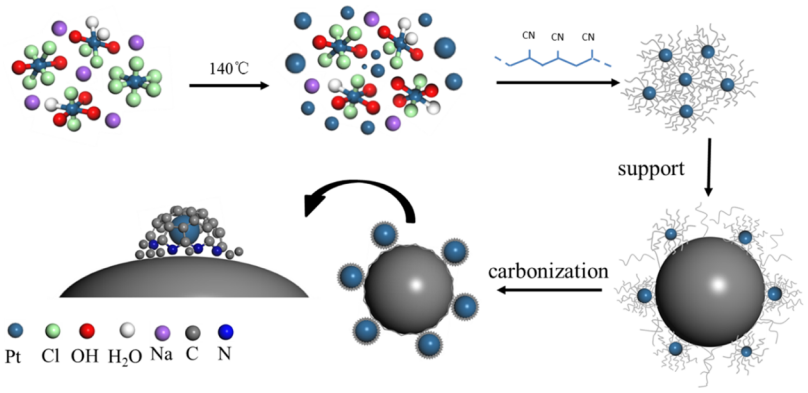

Figure 1. Schematic illustration of the preparation process of the Pt@NC/C catalyst.

the Pt NPs can be stabilized by increasing the interaction between the metal−support.[24]

In this work, based on the advantages of the above-mentioned encapsulated structure, combining the positive influence of nonmetal heteroatom dopants on the activity and stability of Pt catalysts,[4,29] we design a N-doped carbon-encapsulated Pt nanocrystalline structure catalyst fixed firmly on the carbon support, greatly improving the stability of the Pt-based catalyst. Herein, as the cheap polypropylene fiber (PANF) can be converted into a hexagonal N-doped carbon structure after preoxidation and carbonization,[30−34] it is selected as the precursor of the N-doped carbon. Importantly, the fiber structure of PANF is feasible to construct the porous carbon framework, promoting the mass transfer and reducing the occupancy of surface-active sites on Pt NPs. To obtain relatively uniform and ultrasmall Pt NPs, first, Pt colloids are prepared in advance by an ethylene glycol (EG) reduction method.[24,26] As a result, the prepared catalyst (Pt@NC/C) with Pt nanocrystals (3 nm diameter in average size) exhibits higher stability than the commercial Pt/C catalyst (20 wt %, Johnson Matthey Co.) as a control sample.

2. EXPERIMENTAL SECTION

2.1. Synthesis of the Pt@PANF/C Precursor. The synthesis procedures of Pt@NC/C are illustrated in Figure 1. First, 1.5 mg_{Pt} mL^{-1} H_2PtCl_6 EG solution and a certain amount of EG were fully mixed in a three-necked flask. Then, the 0.1 M NaOH aqueous solution was slowly poured into the mixture to adjust the pH to a range of 10−14. The above homogeneous reaction system was heated at 140 °C, and continuously stirred until the color changed from bright yellow to brownish black (about 30 min). This change indicated that a Pt colloidal dispersion was obtained. Subsequently, the *N*,*N*-dimethylformamide solution of PANF was directly added into the above colloidal dispersion and stirred for 1 h to ensure that PANF was sufficiently wrapped on Pt colloids to form a Pt@PANF colloidal dispersion. Simultaneously, 100 mg of Vulcan XC-72 was mixed with 50 mL of EG, and then the suspension was evenly dispersed under an ultrasonic condition. After a while, the above mixture was introduced into the Pt@PANF colloidal dispersion with continuous stirring at 140 °C for 4 h, and subsequently naturally cooled to ambient temperature. As a result, the obtained black suspension was filtered, washed, and the obtained solid powder was completely dried in vacuum at 70 °C to obtain the Pt@PANF/C precursor.

2.2. Preparation of Catalysts. For the sake of obtaining the N-doped carbon structure, the precursor was preoxidized at 320 °C for 60 min, and then subjected to pyrolysis at 720 °C for 90 min. The PANF coated on the Pt particle was then carbonized into a thin porous N-containing carbon framework. The heat treatment process was implemented in nitrogen atmosphere at a heating rate of 5 °C/min, and the sample was cooled to room temperature to acquire the desired Pt@NC/C catalyst powder.

In addition, as presented in Table S1, the exact contents of Pt for Pt@NC/C and Pt/C (as a benchmark, Johnson Matthey Corp.) are 21.10 and 21.49%, respectively, measured by inductively coupled plasma-optical emission spectrometry (ICP, Optima Prodigy 7).

2.3. Structural Characterizations. X-ray diffraction (XRD) patterns were recorded on a rotation anode high-power X-ray diffractometer (RU-200B/D/MAX-RB) with Cu Kα radiation (λ = 1.5418 Å) to obtain the lattice phases of catalysts. Fourier transform infrared (FTIR) spectra were collected by FTIR spectroscopy (Nicolet-6700, U.S.A.) to verify the existence of PANF in the sample. The morphology of Pt/C, Pt@PANF/C, and Pt@NC/C was characterized by a transmission electron microscope (TEM, JEM-2100F) and high-resolution transmission electron microscope ; meanwhile, an energy-dispersive spectrometer was used to visualize the distribution of some elements (such as Pt, N, and C). X-ray photoelectron spectroscopy (XPS), using Mg KR as radiation was employed to determine the type and valence state of the elements in the sample, as well as the interaction of the Pt NP and NC structure.

2.4. Electrochemical Characterizations. Electrochemical measurements were conducted by a traditional three-electrode setup using an AUTO LAB Electrochemical System (Eco Chemie Corp.). Ag/AgCl with saturated KCl and a Pt wire electrode were used as reference and counter electrodes, respectively. Catalyst powders (3 mg), 100 μL of deionized water (R = 18.2 MΩ), 900 μL of isopropyl alcohol, and 20 of μL Nafion (5% DuPont Co., Ltd.) solution were mixed and ultrasonicated for 30 min to obtain a homogeneous catalyst ink. Then, the ink was coated on a glassy carbon rotating disk electrode (0.196 cm^2) as a working electrode. The Pt loading of each working electrode surface was 20 μg cm^{-1}. The electrolyte (0.1 M $HClO_4$ solution) was purged with pure O_2 or N_2 for at least 30 min.

The working electrodes were first electrochemically cleaned by performing cyclic voltammetry (CV) between 0 and 1.2 V (vs RHE) at a sweep rate of 100 mV s^{-1} in the N_2-saturated 0.1 M $HClO_4$ solution before the ORR measurements. Then, CV curves were recorded at 50 mV s^{-1}, which could be generally used to evaluate the electrochemical surface area (ECSA) of Pt catalysts.[23] The ORR polarization curves were obtained in linear sweep voltammetry (LSV) mode with a sweep rate of 5 mV s^{-1} in a potential range of 0−1.2 V (vs RHE) and a rotating speed of 1600 rpm in an O_2-saturated 0.1 M $HClO_4$ solution. The kinetic current at 0.9 V (vs RHE) was determined based on the LSV curve. Furthermore, the mass activity[23] can be calculated from the kinetic current.

An electrochemical accelerated durability test (ADT) was employed to evaluate the long-term stability of catalysts.[35] Eight thousand potential cycles were performed over a potential range of 0.6−1.2 V (vs RHE) with a scan rate of 100 mV s^{-1}. ORR polarization curves of the catalysts were recorded after ADT to investigate the decay of catalyst activity.

DOI: 10.1021/acs.langmuir.8b03947
Langmuir 2019, 35, 2580−2586

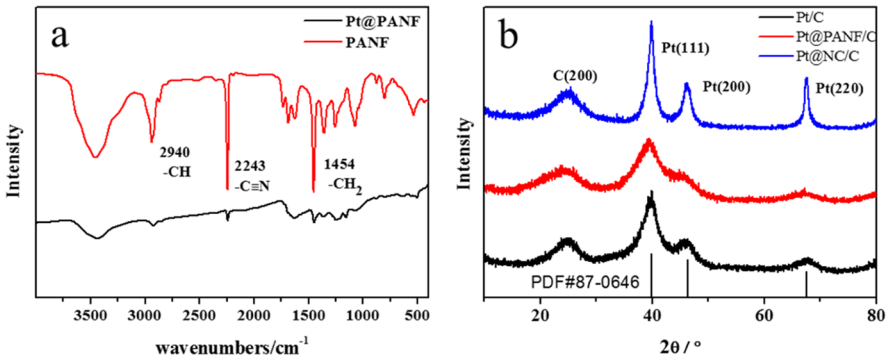

Figure 2. (a) FTIR spectra of PANF and Pt@PANF. (b) XRD patterns of Pt@PANF/C, Pt@NC/C, and Pt/C.

3. RESULTS AND DISCUSSION

As displayed in Figure 2a, FTIR spectra of Pt@PANF and PANF confirm that the PANF is present in the as-prepared Pt@PANF. The characteristic peaks of PANF at 2243 cm^{-1} correspond to the −C≡N stretching vibration peak.[36] The peaks at 1454 and 2940 cm^{-1} are the $-CH_2$ out-of-plane bending vibration peak and −CH asymmetrical stretching vibration peak, respectively. The spectrum of Pt@PANF also reveals similar absorption peaks at the same wavenumber position, proving the presence of PANF wrapped on Pt NPs.

Figure 2b presents XRD patterns of Pt/C, Pt@PANF/C, and Pt@NC/C. The broad peaks at about 24.5° are assigned to the C(002) crystal plane. Three peaks at 2θ = 39.8°, 46.3°, 67.5°, which correspond to the Pt(111), (200), and (220) facets (PDF#87−0646), respectively, reveal that the crystal structure of Pt NPs in these samples is a face-centered cubic structure. The more obvious Pt peaks of Pt@NC/C, compared with the others, indicate that Pt NPs are better crystallized with more regular lattices. This crystalline structure can also be proved by TEM images.

Figure 3 shows the microstructure of Pt@PANF/C and Pt@NC/C, whereas that of Pt/C is presented in Figure S1a. It can be found that most Pt NPs in the three catalysts are highly dispersed on carbon supports. Among them, the unheated Pt@PANF/C presents unclear grain edges (Figures 3a,b and S1b) because of inadequate crystallization and smaller particle size. As for Pt@NC/C, the lattice stripes of Pt NPs are clearer and distinguished, consistent with XRD analysis results, indicating that such Pt particles possess a nanocrystalline structure. Next, 200 randomly selected NPs were counted to obtain an average particle size. The diameter of Pt NPs in Pt@PANF/C, Pt@NC/C, and Pt/C is around 1.3, 3.0, and 2.7 nm (Figure S2), respectively. From the particle size distribution, it is found that Pt@PANF/C possesses the smallest diameter and narrow particle size distribution of Pt NPs. This result can be attributed to the EG reduction method as well as the protection of PANF, through which relatively uniform Pt particles form in colloidal suspension. As shown in Figure 3c,d, after the heat treatment, the size of Pt NPs grows slowly with a crystalline process. A 0.22 nm adjacent lattice spacing of Pt NPs is clearly exhibited in the inset of Figure 3d, corresponding to the Pt(111) crystal planes, which agrees with the XRD result. Then, the 0.34 nm lattice spacing is related to C(200). As indicated in Figure S1c,d, it is proved that PANF is wrapped around Pt NPs as a decoration layer. In the meanwhile, after heat treatment, the carbonized layer of PANF for Pt@NC/C (Figure 3e) indicates the presence of the layered structure on the surface of the Pt NPs. Figure 3f is the

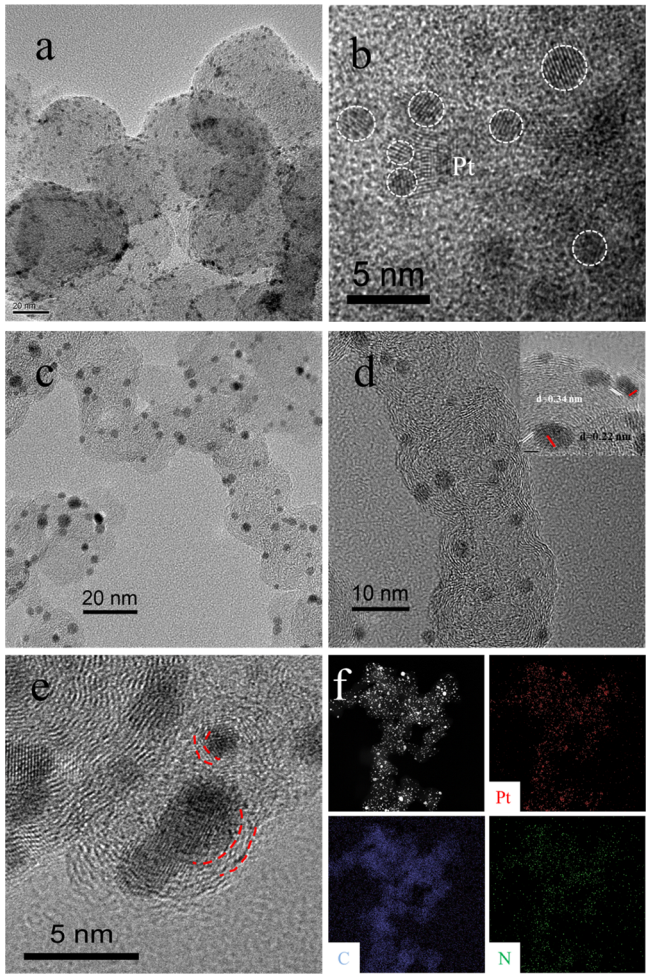

Figure 3. TEM images of Pt@PANF/C (a,b) and Pt@NC/C (c−f). The inset in (d) is the lattice of Pt NPs and the outer carbon structure. (e) Layer structure of Pt@NC/C. TEM images corresponding to EDX patterns of Pt@NC/C (f).

elemental mapping recorded by high angle annular dark field-scanning transmission electron-energy dispersive spectrometer (HAADF−STEM−EDS). It demonstrates the existence of elemental N derived from carbonized PANF along with Pt, and confirms the encapsulation of N-doped carbon with the layer structure on Pt NP surfaces (Figure 3e).

The surface elemental composition and chemical status of catalysts were obtained by XPS (Figure 4). As clearly indicated in Figure 4a, the C 1s signal at 284.2 eV and the Pt 4f, Pt 4d, Pt

DOI: 10.1021/acs.langmuir.8b03947
Langmuir 2019, 35, 2580−2586

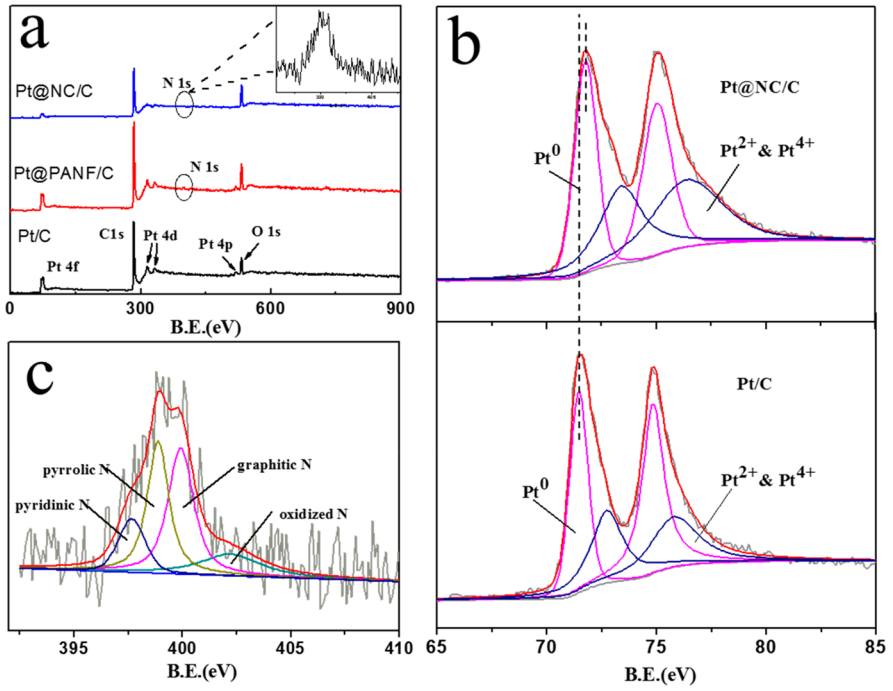

Figure 4. (a) XPS spectra of Pt/C, Pt@PANF/C, and Pt@NC/C; (b) Pt 4f spectra of Pt@NC/C and Pt/C; (c) N 1s spectra of Pt@NC/C.

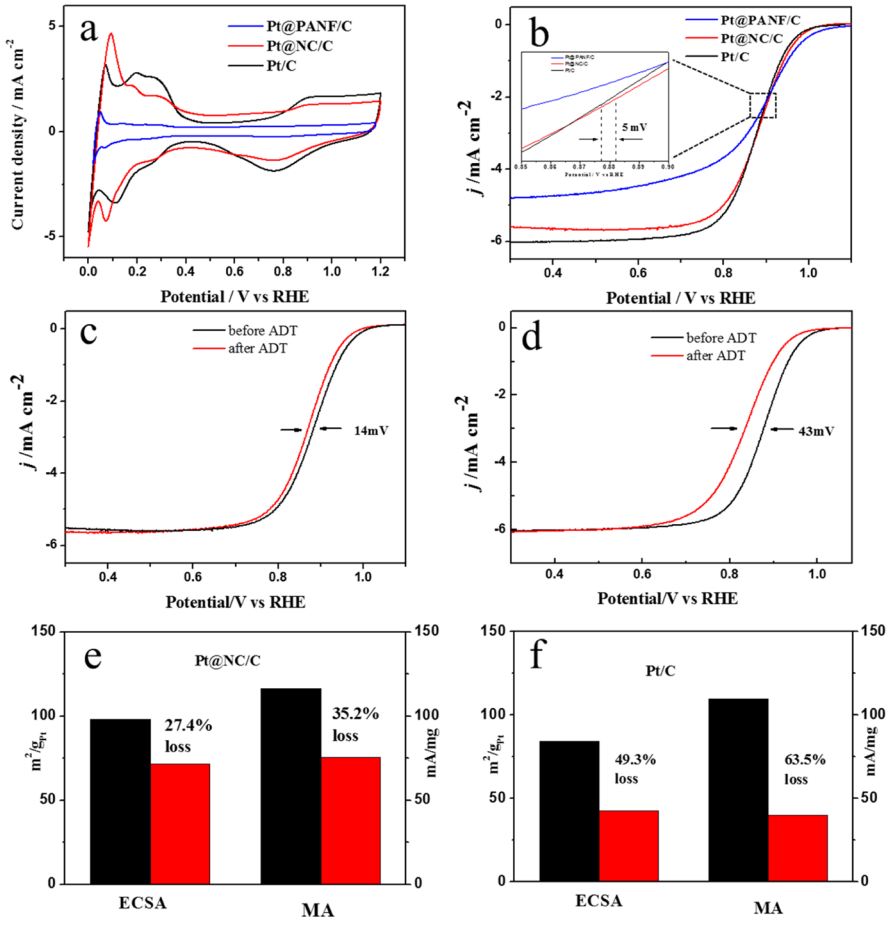

Figure 5. (a) CV and (b) LSV curves of Pt/C, Pt@PANF/C, and Pt@NC/C. The inset of (b) is the change of $E_{1/2}$. Comparison of (c,d) ORR polarization curves, the ECSA and MA loss (e,f) for Pt@NC/C and Pt/C before and after ADT tests. The ORR was tested at a rotating speed of 1600 rpm in an O_2-saturated 0.1 mol L^{-1} $HClO_4$ solution with a sweep rate of 5 mV s^{-1}.

DOI: 10.1021/acs.langmuir.8b03947
Langmuir 2019, 35, 2580−2586

4p, and O 1s signals appear in all three samples. In addition, the peak at 400 eV is from the N 1s signal, which occurs in PANF and N-doped carbon structures. The inset in Figure 4a is the enlarged N signal, which can be deconvoluted into four peaks at 397.7, 398.9, 399.9, and 402.8 eV (Figure 4c), corresponding to pyridinic N, pyrrolic N, graphitic N, and oxidized N,[37,38] respectively. According to recently reported literature,[39,40] the presence of pyridinic-N and graphitic-N in the catalyst is beneficial to improve the ORR performance, as both have lone pairs that can be donated to Pt atoms or can change the distribution of electrons in adjacent atoms. The Pt 4f peak (Figure 4b) can be fitted into $4f_{7/2}$ and $4f_{5/2}$ because of the spin−orbit interaction, which are located at 71.77 and 75.07, 72.92 and 76.24 eV, corresponding to Pt^0 and Pt ion (Pt^{2+} and Pt^{4+}), respectively. Apparently, the Pt^0 binding energy (71.77 eV) of Pt@NC/C is almost same as that of Pt/C (71.44 eV).

The CV curves were recorded in N_2-saturated 0.1 M $HClO_4$ solution between 0 and 1.2 V (vs RHE) at a sweep rate of 50 mV s^{-1}. Figure 5a illustrates that the CV curve of Pt@NC/C is similar to that of Pt/C and has a larger double-layer thickness owing to the N-doped carbon structure derived from carbonized PANF.[40,41] According to the integral area of the hydrogen desorption region, the calculated ECSA of catalysts is 98.3 m^2/g_{Pt} for Pt@NC/C and 84.2 m^2/g_{Pt} for Pt/C. Because of the ultrasmall Pt particle size (less than 1.8 nm)[42] and the presence of outside PANF, the electrochemical properties of Pt@PANF/C are poor (no clear oxidation peak and reduction peak in Figure 5a). Therefore, Pt@PANF/C was excluded from the electrocatalytic analysis below. The ORR polarization curves of Pt/C and Pt@NC/C are displayed in Figure 5b, the inset of which shows the half-wave potential ($E_{1/2}$) for Pt@NC/C is 0.882 V, presenting a 5 mV positive shift compared with Pt/C (0.877 V). The mass activity of the homemade catalyst at 0.9 V calculated from the LSV curve is 116.5 mA/mg (Table S2), higher than that of commercial Pt/C (109.6 mA/mg). Furthermore, a set of LSV curves at different rotating speeds was recorded to investigate the mechanism of the electron transfer process of Pt@NC/C (Figure S3). The calculated average electron transfer number (n) is 3.84 according to K−L plots of Pt@NC/C[37,40] shown in the inset of Figure S3.

An ADT protocol was used to evaluate stabilities of the catalysts. As shown in Figure 5c,d, after 8000 cycles, the half-wave potential for Pt@NC/C only reduces by 14 mV, whereas it is 43 mV for Pt/C. Figure 5e,f corresponds to the decrease of ECSA and mass activity (MA) before and after ADT for Pt@NC/C and Pt/C, respectively. The ECSA loss of Pt@NC/C over 8000 cycles is 27.4%, much lower than that of Pt/C (49.3%). Moreover, the MA loss for the prepared catalyst calculated by LSV curves before and after ADT decreases by 35.2% and by 63.5% for Pt/C. It is obvious that the stability of Pt@NC/C is significantly higher than that of commercial Pt/C. Generally, the decline of the ECSA can be attributed to agglomeration and detachment of Pt NPs.[6] As presented in Figure 6, after ADT, the average diameter of Pt NPs for Pt@NC/C only increases from 3.0 to 5.6 nm, whereas Pt/C has a faster growth rate from 2.7 to 7.2 nm. Also, TEM images show a lesser agglomeration of Pt NPs for Pt@NC/C.

From electrochemical tests, the larger ECSA of Pt@NC/C suggests that the N-doped carbon-encapsulated structure on Pt NPs has no obvious effect on the active sites and mass transfer of reaction species probably owing to the porous and ultrathin

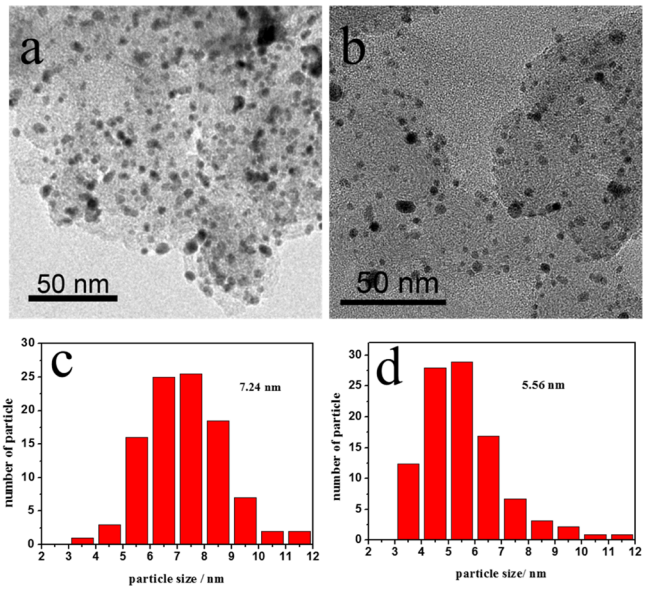

Figure 6. TEM images of Pt/C and Pt@NC/C after ADT. (c,d) Size distribution of Pt NPs for Pt/C and Pt@NC/C after ADT.

properties of the NC framework structure and the ultrasmall crystalline structure with more exposed Pt(111) facets, which ameliorate H absorption on Pt surfaces. Although some surface-active sites of Pt catalysts are possibly covered by C−N layers, the present N-C structure served as another active site is beneficial to adsorption and activation of oxygen. Thus, its catalytic ORR activity does not decrease. It is worth noting that the introduced N-doped modified layer as a protective layer can effectively prevent Pt NPs from migration, agglomeration, or detachment. The result proves that the N-doped carbon layer-encapsulated Pt NPs facilitate the stability of Pt catalysts.

4. CONCLUSIONS

A new N-doped carbon-encapsulated Pt nanocrystalline catalyst (Pt@NC/C) is designed and successfully synthesized by a simple EG reduction method using PANF as the nitrogen−carbon source. The obtained catalyst possesses robust durability and high ORR activity compared with the commercial Pt/C catalysts. The porous N-doped carbon framework structure wrapped Pt NPs not only inhibits the movement of Pt NPs, but also increase the interaction between Pt nanocrystals and supports. Besides, the N−C, as an active site, can improve the electrochemical activity because of synergistic oxygen reduction with Pt NPs. As a result, Pt@NC/C as a unique Pt-based catalyst owns outstanding long-term stability in the case of high ORR activity.

■ ASSOCIATED CONTENT

Supporting Information

The Supporting Information is available free of charge on the ACS Publications website at DOI: 10.1021/acs.langmuir.8b03947.

TEM image of Pt@PANF/C; more TEM images and the size distribution of Pt NPs for Pt/C, Pt@PANF/C, and Pt@NC/C; and a group of CV curves after 2000 of potential cycling by ADT in 0.1 M $HClO_4$ at a scan rate of 50 mV s^{-1} (PDF)

DOI: 10.1021/acs.langmuir.8b03947
Langmuir 2019, 35, 2580−2586

AUTHOR INFORMATION

Corresponding Author

*E-mail: msc@whut.edu.cn. Phone: +86 27 87651837.

ORCID

Daping He: 0000-0002-0284-4990

Shichun Mu: 0000-0003-3902-0976

Notes

The authors declare no competing financial interest.

ACKNOWLEDGMENTS

This work is financially supported by the National Natural Science Foundation of China (NSFC) (grant no. 51672204). We thank the Materials Analysis Center of Wuhan University of Technology for the HRTEM measurement and other test supports.

REFERENCES

(1) Kaewsai, D.; Hunsom, M. Comparative Study of the ORR Activity and Stability of Pt and PtM (M = Ni, Co, Cr, Pd) Supported on Polyaniline/Carbon Nanotubes in A PEM Fuel Cell. *Nanomaterials* **2018**, *8*, 299−319.

(2) Tsai, M.-J.; Hsieh, T.-H.; Wang, Y.-Z.; Ho, K.-S.; Chang, C.-Y. Microwave Assisted Reduction of Pt-catalyst by N-phenyl-p-phenylenediamine for Proton Exchange Membrane Fuel Cells. *Polymers* **2017**, *9*, 104−119.

(3) Chen, S.; Wei, Z.; Qi, X.; Dong, L.; Guo, Y.-G.; Wan, L.; Shao, Z.; Li, L. Nanostructured Polyaniline-Decorated Pt/C@PANI Core-Shell Catalyst with Enhanced Durability and Activity. *J. Am. Chem. Soc.* **2012**, *134*, 13252−13255.

(4) Nie, Y.; Chen, S.; Ding, W.; Xie, X.; Zhang, Y.; Wei, Z. Pt/C Trapped in Activated Graphitic Carbon Layers as a Highly Durable Electrocatalyst for the Oxygen Reduction Reaction. *Chem. Commun.* **2014**, *50*, 15431−15434.

(5) Meier, J. C.; Galeano, C.; Katsounaros, I.; Topalov, A. A.; Kostka, A.; Schüth, F.; Mayrhofer, K. J. J. Degradation Mechanisms of Pt/C Fuel Cell Catalysts under Simulated Start-Stop Conditions. *ACS Catal.* **2012**, *2*, 832−843.

(6) Chung, D. Y.; Yoo, J. M.; Sung, Y.-E. Highly Durable and Active Pt-Based Nanoscale Design for Fuel-Cell Oxygen-Reduction Electrocatalysts. *Adv. Mater.* **2018**, *30*, 1704123.

(7) Kou, Z.; Cheng, K.; Wu, H.; Sun, R.; Guo, B.; Mu, S. Observable Electrochemical Oxidation of Carbon Promoted by Platinum Nanoparticles. *ACS Appl. Mater. Interfaces* **2016**, *8*, 3940−3947.

(8) Castanheira, L.; Silva, W. O.; Lima, F. H. B.; Crisci, A.; Dubau, L.; Maillard, F. Carbon Corrosion in Proton-Exchange Membrane Fuel Cells: Effect of the Carbon Structure, the Degradation Protocol, and the Gas Atmosphere. *ACS Catal.* **2015**, *5*, 2184−2194.

(9) Cheng, N.; Liu, J.; Banis, M. N.; Geng, D.; Li, R.; Ye, S.; Knights, S.; Sun, X. High Stability and Activity of Pt Electrocatalyst on Atomic Layer Deposited Metal Oxide/Nitrogen-Doped Graphene Hybrid Support. *Int. J. Hydrogen Energy* **2014**, *39*, 15967−15974.

(10) Merte, L. R.; Behafarid, F.; Miller, D. J.; Friebel, D.; Cho, S.; Mbuga, F.; Sokaras, D.; Alonso-Mori, R.; Weng, T.-C.; Nordlund, D.; Nilsson, A.; Cuenya, R. B. Electrochemical Oxidation of Size-Selected Pt Nanoparticles Studied Using in Situ High-Energy-Resolution X-ray Absorption Spectroscopy. *ACS Catal.* **2012**, *2*, 2371−2376.

(11) Zhdanov, V. P.; Schweinberger, F. F.; Heiz, U.; Langhammer, C. Ostwald Ripening of Supported Pt Nanoclusters with Initial Size-Selected Distributions. *Chem. Phys. Lett.* **2015**, *631-632*, 21−25.

(12) Cognard, G.; Ozouf, G.; Beauger, C.; Berthomé, G.; Riassetto, D.; Dubau, L.; Chattot, R.; Chatenet, M.; Maillard, F. Benefits and Limitations of Pt Nanoparticles Supported on Highly Porous Antimony-Doped Tin Dioxide Aerogel as Alternative Cathode Material for Proton-Exchange Membrane Fuel Cells. *Appl. Catal., B Enviro.* **2017**, *201*, 381−390.

(13) Gimenez-Lopez, M. d. C.; Kurtoglu, A.; Walsh, D. A.; Khlobystov, A. N. Extremely Stable Platinum-Amorphous Carbon Electrocatalyst within Hollow Graphitized Carbon Nanofibers for the Oxygen Reduction Reaction. *Adv. Mater.* **2016**, *28*, 9103−9108.

(14) He, D.; Zeng, C.; Xu, C.; Cheng, N.; Li, H.; Mu, S.; Pan, M. Polyaniline-Functionalized Carbon Nanotube Supported Platinum Catalysts. *Langmuir* **2011**, *27*, 5582−5588.

(15) Song, Z.; Banis, M. N.; Zhang, L.; Wang, B.; Yang, L.; Banham, D.; Zhao, Y.; Liang, J.; Zheng, M.; Li, R.; Ye, S.; Sun, X. Origin of Achieving the Enhanced Activity and Stability of Pt Electrocatalysts with Strong Metal-Support Interactions via Atomic Layer Deposition. *Nano Energy* **2018**, *53*, 716−725.

(16) Tian, X.; Luo, J.; Nan, H.; Zou, H.; Chen, R.; Shu, T.; Li, X.; Li, Y.; Song, H.; Liao, S.; Adzic, R. R. Transition Metal Nitride Coated with Atomic Layers of Pt as a Low-Cost, Highly Stable Electrocatalyst for the Oxygen Reduction Reaction. *J. Am. Chem. Soc.* **2016**, *138*, 1575−1583.

(17) Chen, Q.; Cao, Z.; Du, G.; Kuang, Q.; Huang, J.; Xie, Z.; Zheng, L. Excavated Octahedral Pt-Co Alloy Nanocrystals Built with Ultrathin Nanosheets as Superior Multifunctional Electrocatalysts for Energy Conversion Applications. *Nano Energy* **2017**, *39*, 582−589.

(18) Peng, X.; Zhao, S.; Omasta, T. J.; Roller, J. M.; Mustain, W. E. Activity and Durability of Pt-Ni Nanocage Electocatalysts in Proton Exchange Membrane Fuel Cells. *Appl. Catal., B* **2016**, *203*, 927−935.

(19) Zhang, N.; Bu, L.; Guo, S.; Guo, J.; Huang, X. Screw Thread-Like Platinum-Copper Nanowires Bounded with High-Index Facets for Efficient Electrocatalysis. *Nano Lett.* **2016**, *16*, 5037−5043.

(20) Song, Z.; Wang, B.; Cheng, N.; Yang, L.; Banham, D.; Li, R.; Ye, S.; Sun, X. Atomic Layer Deposited Tantalum Oxide to Anchor Pt/C for a Highly Stable Catalyst in PEMFCs. *J. Mater. Chem. A* **2017**, *5*, 9760−9767.

(21) Sivanantham, A.; Ganesan, P.; Estevez, L.; McGrail, B. P.; Motkuri, R. K.; Shanmugam, S. A Stable Graphitic, Nanocarbon-Encapsulated, Cobalt-Rich Core-Shell Electrocatalyst as an Oxygen Electrode in a Water Electrolyzer. *Adv. Energy Mater.* **2018**, *8*, 1702838.

(22) Cheng, N.; Banis, M. N.; Liu, J.; Riese, A.; Li, X.; Li, R.; Ye, S.; Knights, S.; Sun, X. Extremely Stable Platinum Nanoparticles Encapsulated in a Zirconia Nanocage by Area-Selective Atomic Layer Deposition for the Oxygen Reduction Reaction. *Adv. Mater.* **2014**, *27*, 277−281.

(23) Ye, B.; Cheng, K.; Li, W.; Liu, J.; Zhang, J.; Mu, S. Polyaniline and Perfluorosulfonic Acid Co-stabilized Metal Catalysts for Oxygen Reduction Reaction. *Langmuir* **2017**, *33*, 5353−5361.

(24) He, D.; Kou, Z.; Xiong, Y.; Cheng, K.; Chen, X.; Pan, M.; Mu, S. Simultaneous Sulfonation and Reduction of Graphene Oxide as Highly Efficient Supports for Metal Nanocatalysts. *Carbon* **2014**, *66*, 312−319.

(25) Mu, S.; Chen, X.; Sun, R.; Liu, X.; Wu, H.; He, D.; Cheng, K. Nano-Size Boron Carbide Intercalated Graphene as High Performance Catalyst Supports and Electrodes for PEM Fuel Cells. *Carbon* **2016**, *103*, 449−456.

(26) Cheng, K.; Kou, Z.; Zhang, J.; Jiang, M.; Wu, H.; Hu, L.; Yang, X.; Pan, M.; Mu, S. Ultrathin Carbon Layer Stabilized Metal Catalysts towards Oxygen Reduction. *J. Mater. Chem. A* **2015**, *3*, 14007−14014.

(27) Yang, H.; Zhang, Y.; Hu, F.; Wang, Q. Urchin-like CoP Nanocrystals as Hydrogen Evolution Reaction and Oxygen Reduction Reaction Dual-Electrocatalyst with Superior Stability. *Nano Lett.* **2015**, *15*, 7616−7620.

(28) Jiang, S.; Ithisuphalap, K.; Zeng, X.; Wu, G.; Yang, H. 3D Porous Cellular NiCoO2/Graphene Network as a Durable Bifunctional Electrocatalyst for Oxygen Evolution and Reduction Reactions. *J. Power Sources* **2018**, *399*, 66−75.

(29) Zhou, Y.; Neyerlin, K.; Olson, T. S.; Pylypenko, S.; Bult, J.; Dinh, H. N.; Gennett, T.; Shao, Z.; O'Hayre, R. Enhancement of Pt and Pt-Alloy Fuel Cell Catalyst Activity and Durability via Nitrogen-Modified Carbon Supports. *Energy Environ. Sci.* **2010**, *3*, 1437−1446.

(30) Ye, S.; Vijh, A. K.; Dao, L. H. Oxygen Reduction on a New Electrocatalyst Based on Highly Porous Carbonized Polyacrylonitrile

DOI: 10.1021/acs.langmuir.8b03947
Langmuir 2019, 35, 2580−2586

Microcellular Foam with Very Low Platinum Loading. *J. Electroanal. Chem.* **1996**, *415*, 115−121.
(31) Ye, S.; Vijh, A. K.; Dao, L. H. Fractal Dimension of Platinum Particles Dispersed in Highly Porous Carbonized Polyacrylonitrile Microcellular Foam. *J. Electrochem. Soc.* **1997**, *144*, 1734−1738.
(32) Ji, M.; Wang, C.; Bai, Y.; Yu, M.; Wang, Y. Structural Evolution of Polyacrylonitrile Precursor Fibers during Preoxidation and Carbonization. *Polym. Bull.* **2007**, *59*, 527−536.
(33) Gissinger, J. R.; Pramanik, C.; Newcomb, B.; Kumar, S.; Heinz, H. Nanoscale Structure-Property Relationships of Polyacrylonitrile/CNT Composites as a Function of Polymer Crystallinity and CNT Diameter. *ACS Appl. Mater. Interfaces* **2017**, *10*, 1017−1027.
(34) Nataraj, S. K.; Yang, K. S.; Aminabhavi, T. M. Polyacrylonitrile-based nanofibers-A state-of-the-art review. *Prog. Polym. Sci.* **2012**, *37*, 487−513.
(35) Zhang, Y.; Chen, S.; Wang, Y.; Ding, W.; Wu, R.; Li, L.; Qi, X.; Wei, Z. Study of the Degradation Mechanisms of Carbon-Supported Platinum Fuel Cells Catalyst via Different Accelerated Stress Test. *J. Power Sources* **2015**, *273*, 62−69.
(36) Lachat, V.; Varshney, V.; Dhinojwala, A.; Yeganeh, M. S. Molecular Origin of Solvent Resistance of Polyacrylonitrile. *Macromolecules* **2009**, *42*, 7103−7107.
(37) Zhu, J.; Zhou, H.; Zhang, C.; Zhang, J.; Mu, S. Dual Active Nitrogen Doped Hierarchical Porous Hollow Carbon Nanospheres as an Oxygen Reduction Electrocatalyst for Zinc-Air Batteries. *Nanoscale* **2017**, *9*, 13257−13263.
(38) Brandiele, R.; Durante, C.; Zerbetto, M.; Vicentini, N.; Kosmala, T.; Badocco, D.; Pastore, P.; Rizzi, G. A.; Isse, A. A.; Gennaro, A. Probing the Correlation between Pt-support Interaction and Oxygen Reduction Reaction Activity in Mesoporous Carbon Materials Modified with Pt-N Active Sites. *Electrochim. Acta* **2018**, *277*, 287−300.
(39) Perazzolo, V.; Brandiele, R.; Durante, C.; Zerbetto, M.; Causin, V.; Rizzi, G. A.; Cerri, I.; Granozzi, G.; Gennaro, A. Density Functional Theory (DFT) and Experimental Evidences of Metal-Support Interaction in Platinum Nanoparticles Supported on Nitrogen- and Sulfur-Doped Mesoporous Carbons: Synthesis, Activity, and Stability. *ACS Catal.* **2018**, *8*, 1122−1137.
(40) Perini, L.; Durante, C.; Favaro, M.; Perazzolo, V.; Agnoli, S.; Schneider, O.; Granozzi, G.; Gennaro, A. Metal-Support Interaction in Platinum and Palladium Nanoparticles Loaded on Nitrogen-Doped Mesoporous Carbon for Oxygen Reduction Reaction. *ACS Appl. Mater. Interfaces* **2015**, *7*, 1170−1179.
(41) Gao, Z.; Wang, F.; Chang, J.; Wu, D.; Wang, X.; Wang, X.; Xu, F.; Gao, S.; Jiang, K. Chemically Grafted Graphene-Polyaniline Composite for Application in Supercapacitor. *Electrochim. Acta* **2014**, *133*, 325−334.
(42) Shao, M.; Peles, A.; Shoemaker, K. Electrocatalysis on Platinum Nanoparticles: Particle Size Effect on Oxygen Reduction Reaction Activity. *Nano Lett.* **2011**, *11*, 3714−3719.

DOI: 10.1021/acs.langmuir.8b03947
Langmuir 2019, 35, 2580−2586